Available online at www.sciencedirect.com
ScienceDirect
Journal of the European Ceramic Society 30 (2010) 1731–1736
www.elsevier.com/locate/jeurceramsoc

Effects of packing fraction and bond valence on microwave dielectric properties of $A^{2+}B^{6+}O_4$ (A^{2+}: Ca, Pb, Ba; B^{6+}: Mo, W) ceramics

Eung Soo Kim [a,*], Byung Sam Chun [a], Robert Freer [b], Robert J. Cernik [b]

[a] *Department of Materials Engineering, Kyonggi University, 94-6 Yiei-dong, Youngtong-gu, Suwon 443-760, Republic of Korea*
[b] *Materials Science Centre, University of Manchester, Manchester M1 7HS, UK*

Received 20 September 2009; received in revised form 29 November 2009; accepted 30 December 2009
Available online 25 January 2010

Abstract

Microwave dielectric properties of $A^{2+}B^{6+}O_4$ (A^{2+}: Ca, Pb, Ba; B^{6+}: Mo, W) ceramics were investigated as a function of packing fraction and bond valence. For $A^{2+}B^{6+}O_4$ specimens sintered at 800–1100 °C for 3 h, a single phase with a tetragonal scheelite structure was detected, and the theoretical density was higher than 93% throughout the composition. Although the ionic polarizability of Ba^{2+} ion was larger than that of Ca^{2+} ion, the dielectric constant (K) of $BaB^{6+}O_4$ showed a smaller value than that of $CaB^{6+}O_4$. These results could be attributed to changes of the packing fraction due to the effective ionic size. The $Q{\cdot}f$ value was largely dependent on the packing fraction, as well as the percentages of theoretical density. The temperature coefficients of the resonant frequencies (TCFs) of the specimens were affected by the bond valence of oxygen. The specimens of $CaMoO_4$ sintered at 1000 °C for 3 h showed the K of 10.8, $Q{\cdot}f$ of 76,990 GHz and TCF of −22.8 ppm/°C, respectively.

Keywords: Scheelite structure; Dielectric properties; Packing fraction; Bond valence; Sintering

1. Introduction

During the past couple of decades, IC (Integrated Circuit) technologies have been very successfully developed to meet demand by integrating an increasingly higher number of transistors on the chip, and most electronic systems have been compacted while offering high performance and numerous functions. These integration activities will be accelerated and the working frequencies will be higher in the future (3G Mobile (2.5 GHz), Bluetooth (2.5 GHz), GPS (Global Positioning System) (12.6 GHz), LMDS (Local Multipoint Distribution Services) (24–40 GHz), Automotive (77 GHz)).

With tremendous demand for immediate entertainment, instant access to information, and communications anywhere at any time, dielectric materials for technologies related to the integration of passives have been researched for the fabrication of microelectronic components for use in electronic systems and devices. Applicable material systems for integration technologies, MMIC (Monolithic Microwave Integrated Circuits) technology of thin film, MCIC (Multilayer Ceramic Integrated Circuits) technology based on LTCC (low-temperature co-fired ceramics),[1] and Embedded Passives technology of ceramic–polymer composites based on a multilayer PCB (Printed Circuit Board)[2] are strictly restricted, and several approaches[3] and modifications[4] such as circuit technology and process improvements have been undertaken to overcome these limitations. Most investigations on material systems for GHz application are mainly based on empirical approaches, such as the addition of materials[5] and/or formation of solid solutions[6] with suitable dielectric properties to the target, and the changes of dielectric properties have been explained by the dielectric mixing rule[7] and structural change.[8]

Due to the nature of materials, their dielectric properties are strongly dependent on the chemical nature of constituent ions, the distance between cations and anions and the structural characteristics originating from the bonding type as well as the composition of materials. The fundamental relationships between the structural characteristics and the dielectric properties should also be identified in order to effectively seek out new dielectric materials for GHz applications. Several types of material system such as AO_2, ABO_3 and $A(B, B')O_3$ have been investigated to search the relationships between

* Corresponding author. Tel.: +82 31 249 9764; fax: +82 31 244 6300.
E-mail address: eskim@kyonggi.ac.kr (E.S. Kim).

0955-2219/$ – see front matter © 2010 Elsevier Ltd. All rights reserved.
doi:10.1016/j.jeurceramsoc.2009.12.018

microwave dielectric properties and the characteristics of crystal structure.[9–11] Therefore, the present study focuses on the dependence of the microwave dielectric properties of scheelite compound, $A^{2+}B^{6+}O_4$ (A^{2+}: Ca, Pb, Ba; B^{6+}: Mo, W) ceramics on its structural characteristics.

2. Experimental procedure

$A^{2+}B^{6+}O_4$ (A^{2+}: Ca, Pb, Ba; B^{6+}: Mo, W) was prepared by the conventional mixed oxide method. $CaCO_3$, PbO, $BaCO_3$, MoO_3, and WO_3 powders with high-purity (99.9%) were used as starting materials. They were milled using ZrO_2 balls for 24 h in ethanol and then dried. The dried powders were calcined from 400 to 700 °C for 3 h, and then milled again for 24 h. The milled powders were pressed into 10 mm diameter disks under pressure of 1500 kg/cm^2 isostatically. These disks were sintered from 800 to 1100 °C for 3 h in air.

Crystalline phases of the specimens were identified with powder X-ray diffraction patterns (D/Max-3C, Rigaku, Japan). Microstructure was observed using a scanning electron microscope (JSM6500F, JEOL, Japan). Bond lengths of the specimens were obtained from geometric calculations based on Rietveld refinements of XRD patterns. The dielectric constant (K) and Q value at frequencies of 10–11 GHz were measured by the post-resonant method developed by Hakki and Coleman.[12] TCF was measured by the cavity method[13] at frequencies of 10–11 GHz and a temperature range of 25–80 °C.

3. Results and discussion

3.1. Crystal structure and physical properties

$A^{2+}B^{6+}O_4$ (A^{2+}: Ca, Pb, Ba; B^{6+}: Mo, W) scheelite compound crystallize in tetragonal symmetry with four molecules per unit cell (space group: $I4_1/a$), as shown in Fig. 1. A-site and B-site ions are positioned at the corner and face-center of the primitive unit cell, respectively, while the oxygen ion is located at the corner of a tetrahedron that also include two A-site ions and one B-site ion. Each B-site ion is surrounded by four oxygen ions, while eight oxygen ions are near to the A-site ion due to the ionic size differences between the A-site and B-site ions. The coordination number of oxygen ion, i.e., 3, agrees well with the neutrality condition of Pauling's law. A- and B-site bond strengths, defined by the ionic valence over the coordination number, are 2/8 and 6/4, respectively. The total charge of cations to oxygen ions is the summation of the bond strength multiplied by the coordination number on each cation site: $(2/8 \times 2) + (6/4 \times 1) = 2$, which corresponds to the charge of oxygen ion. Therefore, the coordination numbers of A- and B-sites and oxygen ions are 8, 4, and 3, respectively. Each ionic position in a unit cell could be described as follows[14]: A-site cation ((0, 0, 1/2), (1/2, 0, 1/4), (1/2, 1/2, 0), (0, 1/2, 3/4)), B-site cation ((0, 0, 0), (0, 1/2, 1/4), (1/2, 1/2, 1/2), (1/2, 0, 3/4)), Oxygen ion ((x, y, z), $(-x, -y, z)$, $(x, 1/2+y, 1/4-z)$, $(-x, 1/2-y, 1/4-z)$, $(-y, x, -z)$, $(y, -x, -z)$, $(-y, 1/2+x, 1/4+z)$, $(y, 1/2-x, 1/4+z)$, ($x = 0.241$, $y = 0.151$, $z = 0.081$)).[14]

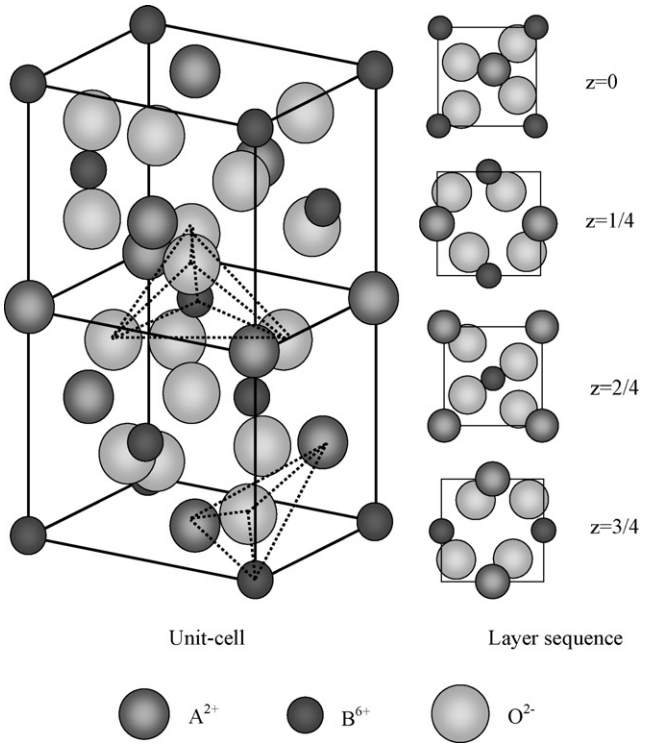

Fig. 1. Crystal structure of $A^{2+}B^{6+}O_4$ scheelite compund.

Assuming a hard sphere of ions, the bond lengths from the A- and B-site cations to oxygen ions could also be obtained from each ionic position and lattice parameters based on geometry, as shown in Eqs. (1)–(4): there are eight bond lengths for the A-site cation to oxygen ion ($d_{A–O}$), where four of the bond lengths are identical, and two sets of different bond lengths, while four bond lengths for the B-site cation to oxygen ion ($d_{B–O}$) are identical.

Four of bond lengths $d_{A–O}$

$$= \sqrt{\left\{\left(\frac{1}{2} - x\right) \times a\right\}^2 + \left\{\left(\frac{1}{2} - y\right) \times a\right\}^2 + (z \times c)^2} \quad (1)$$

Two of bond lengths $d_{A–O}$

$$= \sqrt{\left\{\left(\frac{1}{2} - x\right) \times a\right\}^2 + (y \times a)^2 \left\{\left(\frac{1}{4} - z\right) \times c\right\}^2} \quad (2)$$

Two of bond lengths $d_{A–O}$

$$= \sqrt{\left\{\left(\frac{1}{2} - \mathbf{y}\right) \times a\right\}^2 + (x \times a)^2 \left\{\left(\frac{1}{4} - z\right) \times c\right\}^2} \quad (3)$$

Four of bond lengths $d_{B\text{-}O}$

$$= \sqrt{(x \times a)^2 + (y \times a)^2 + (z \times c)^2} \quad (4)$$

where a and c are lattice parameters, and $x = 0.241$, $y = 0.151$, and $z = 0.081$ are parameters for the position of the oxygen ion, respectively.

Table 1
Physical properties of $A^{2+}B^{6+}O_4$ scheelite compounds.

Compounds	Calcination/sintering temperature (°C)	Lattice *a* (Å)	Parameter *c* (Å)	Sintered density (g/cm^3)	Theoretical density (%)
$CaMoO_4$	600/1000	5.2340	11.4584	4.158	98.2
$PbMoO_4$	400/850	5.4422	12.1237	6.436	94.8
$BaMoO_4$	450/800	5.5888	12.8412	4.684	95.2
$CaWO_4$	700/1100	5.2465	11.4008	5.990	98.3
$PbWO_4$	550/850	5.4761	12.0764	8.090	96.9
$BaWO_4$	600/850	5.6218	12.7359	5.932	93.3

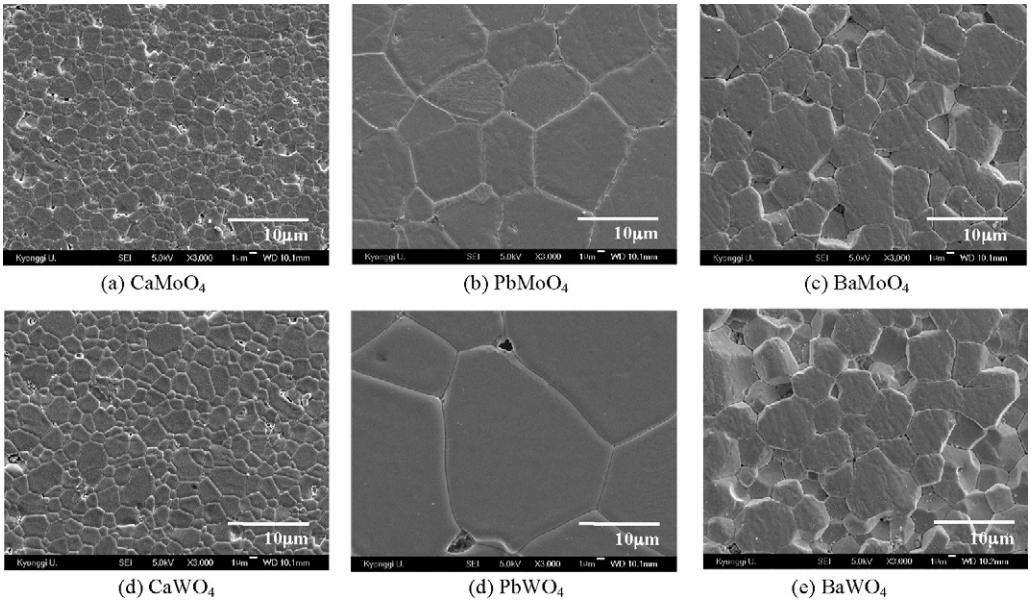

Fig. 2. SEM micrographs of $A^{2+}B^{6+}O_4$ scheelite compound.

From the X-ray diffraction (XRD) patterns of $A^{2+}B^{6+}O_4$ (A^{2+}: Ca, Pb, Ba; B^{6+}: Mo, W) compounds sintered from 800 to 1100 °C for 3 h, a single phase with a tetragonal scheelite structure was confirmed throughout the composition. Due to the increase of effective ionic radius of the A-site ion in $A^{2+}B^{6+}O_4$ scheelite (Ca^{2+} = 1.12 Å, Pb^{2+} = 1.29 Å, and Ba^{2+} = 1.42 Å at CN = 8),[15] the lattice parameters were changed as shown in Table 1. Also, the theoretical density of the sintered specimens was higher than 93%.

Fig. 2 shows the microstructure of the specimens sintered from 800 to 1100 °C for 3 h. A well-densified microstructure was developed and there was no secondary phase for the entire composition, which agrees with the density results. Grain size of $A^{2+}WO_4$ was slightly larger than that of $A^{2+}MoO_4$, while the specimens showed difference in grain size with the A-site cation of $A^{2+}B^{6+}O_4$ ceramics, presumptively due to the difference of grain growth behavior based on the lower melting points of $PbWO_4$ (1123 °C) and $PbMoO_4$ (1060 °C) than those of $CaWO_4$ (1650 °C), $CaMoO_4$ (1430 °C), $BaWO_4$ (1470 °C) and $BaMoO_4$ (1460 °C); $PbB^{6+}O_4$ showed larger grain size than $BaB^{6+}O_4$ and/or $CaB^{6+}O_4$.

4. Microwave dielectric properties

Microwave dielectric properties of $A^{2+}B^{6+}O_4$ specimens calcined and sintered at each optimized temperature are shown in Table 2. Comparing to the previous reports for AWO_4 and $AMoO_4$ (A = Ca, Sr, Ba), the $Q{\cdot}f$ values are slightly smaller and TCFs are larger than those of previous reports.[16,17] These results are possibly due to the differences of processing temperatures

Table 2
Microwave dielectric properties of $A^{2+}B^{6+}O_4$ scheelite compounds.

Compounds	Calcination/sintering temperature (°C)	*K*	$Q{\cdot}f$ (GHz)	TCF (ppm/°C)
$CaMoO_4$	600/1000	10.8	76,990	−22.8
$PbMoO_4$	400/850	25.4	35,150	−20.6
$BaMoO_4$	450/800	9.2	26,580	−16.9
$CaWO_4$	700/1100	10.4	76,550	−24.4
$PbWO_4$	550/850	21.6	34,500	−22.2
$BaWO_4$	600/850	8.2	21,120	−17.7

such as calcination and sintering temperatures. The dielectric constant (K) and $Q{\cdot}f$ value of the $A^{2+}MoO_4$ show larger values than those of $A^{2+}WO_4$ for the same A-site cations, while the microwave dielectric properties of the specimens were strongly dependent on the type of A-site cations of $A^{2+}B^{6+}O_4$ compound.

At microwave frequencies, the dielectric constant (K) and $Q{\cdot}f$ values are dependent on intrinsic factors, ionic polarizabilities, and structural lattice vibrations, respectively, as well as extrinsic factors such as density, microstructure, and the secondary phases.[18] For these specimens of scheelite compounds, the effects of density and the secondary phase could be neglected due to the higher density above the theoretical density of 93% and the absence of detection of secondary phases through the entire composition.

As for the dielectric constant (K), $PbB^{6+}O_4$ showed a larger dielectric constant than $CaB^{6+}O_4$ and/or $BaB^{6+}O_4$ due to the larger ionic polarizability of Pb^{2+} (6.58 Å) relative to Ca^{2+} (3.16 Å) and/or Ba^{2+} (6.40 Å).[19] However, K of $CaB^{6+}O_4$ was larger than that of $BaB^{6+}O_4$, even though the ionic polarizability of the specimens with Ca^{2+} was smaller than those with Ba^{2+}. There is another factor affecting the dielectric constant of the specimens.

Generally, the specimens with large K show a small $Q{\cdot}f$ value, and the intrinsic factor on $Q{\cdot}f$ is the minimum loss related with lattice anharmonicity that can be expected for a particular crystal structure.[18] $Q{\cdot}f$ values of $CaB^{6+}O_4$ were larger than those of $BaB^{6+}O_4$, even though the dielectric constant of the specimens with Ba^{2+} was smaller than those with Ca^{2+}. In addition, the $Q{\cdot}f$ value of $BaMoO_4$ was lower than that of $PbMoO_4$, even though the dielectric constant of $PbMoO_4$ was higher than that of $BaMoO_4$ with a similar theoretical density, as shown in Tables 1 and 2.

Therefore, the microwave dielectric properties were strongly dependent on the structural characteristics. The structural characteristics could be evaluated by the packing fraction and bond valence, since these parameters are a function of unit cell volume, effective ionic size, and bond strength, respectively.

Based on crystal structural considerations, the packing fraction, defined by the summation of the volume of packed ions over the volume of a primitive unit cell, could be obtained from Eq. (5) for an $A^{2+}B^{6+}O_4$ scheelite compound:

$$\begin{aligned}\text{packing fraction (\%)} &= \frac{\text{volume of packed ions}}{\text{volume of primitive unit cell}} \\ &= \frac{\text{volume of packed ions}}{\text{volume of unit cell}} \times Z \\ &= \frac{4\pi/3 \times (r_A^3 + r_B^3 + 4 \times r_o^3)}{a^2 \times c} \times 4 \\ &= \frac{4\pi/3 \times (r_A^3 + r_B^3 + 4 \times r_o^3) \times 4}{a^2 \times c} \end{aligned} \quad (5)$$

where V_A, V_B, and V_O are the volume of ions at each site, r_A, r_B and r_O are the effective ionic radii at each coordination number, a and c are lattice parameters, and $Z = 4$ for a tetragonal scheelite compound.

As shown in Table 3, packing fractions of the scheelite compound were obtained from Eq. (5), and the dependence of the $Q{\cdot}f$ value of the scheelite compound on the packing fraction is clearly confirmed in Fig. 3.

Another important dielectric property for GHz applications is the temperature coefficient of resonant frequency (TCF), which determines the thermal stability of materials and devices. TCF of materials basically results from the temperature dependence of the dielectric constant (TCK) related with the chemical nature of constituent ions, the distance between cations and anions, and the structural characteristics originating from the bonding type. These structural characteristics could be evaluated by the bond valence of ions, as the present authors previously demonstrated these relationships between TCF and bond valance for perovskite systems.[11]

From each bond length for A- and B- site cations to oxygen ions obtained from Eqs. (1) and (4), and bond valence parameters[20] for each ion, the bond valence of ions composing a unit cell was calculated by Eqs. (6) and (7):

$$V_i = \sum_j v_{ij} \quad (6)$$

$$v_{ij} = \exp\left\{\frac{(R_{ij} - d_{ij})}{b}\right\} \quad (7)$$

where R_{ij} is the bond valence parameter, d_{ij} is the length of a bond between atoms i and j, and b is commonly taken to be a universal constant equal to 0.37 Å.

Table 4 shows the bond valence of the ions of each site for $A^{2+}B^{6+}O_4$ scheelite compounds. For the specimens with the same A-site ions, the bond valence of the A-site ions (V_A) decreased if the bond valence of the B-site ions (V_B) increased.

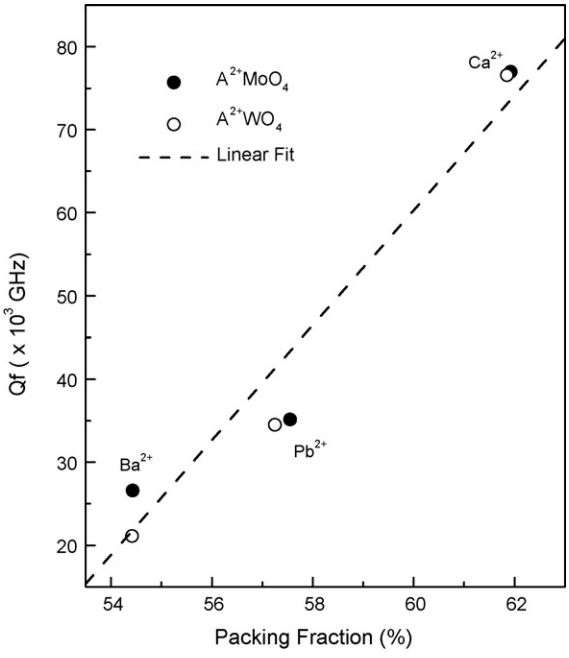

Fig. 3. Dependence of $Q{\cdot}f$ on packing fraction in $A^{2+}B^{6+}O_4$ scheelite compounds.

Table 3
Packing fraction of $A^{2+}B^{6+}O_4$ scheelite compounds.

Compounds	r_A (Å) (CN = 8)	r_B (Å) (CN = 4)	r_O (Å) (CN = 3)	Unit cell volume (Å^3)	Z	Packing fraction (%)
$CaMoO_4$	1.12	0.41	1.36	313.90	4	61.6
$PbMoO_4$	1.29	0.41	1.36	359.07	4	57.3
$BaMoO_4$	1.42	0.41	1.36	401.09	4	54.3
$CaWO_4$	1.12	0.42	1.36	313.82	4	61.6
$PbWO_4$	1.29	0.42	1.36	362.14	4	56.8
$BaWO_4$	1.42	0.42	1.36	402.51	4	54.1

Table 4
Bond valence of $A^{2+}B^{6+}O_4$ scheelite compounds.

Compounds	R_A	R_B	4-($d_{A–O}$)	2-($d_{A–O}$)	2-($d_{A–O}$)	4-($d_{B–O}$)	V_A	V_B	V_O
$CaMoO_4$	1.967	1.907	2.457	2.492	2.653	1.754	1.861	6.045	1.977
$PbMoO_4$	2.112	1.907	2.561	2.619	2.785	1.833	2.021	4.886	1.727
$BaMoO_4$	2.290	1.907	2.642	2.742	2.909	1.900	2.509	4.082	1.648
$CaWO_4$	1.967	1.921	2.460	2.487	2.649	1.755	1.862	6.269	2.033
$PbWO_4$	2.112	1.921	2.573	2.619	2.787	1.839	1.981	4.991	1.743
$BaWO_4$	2.290	1.921	2.652	2.734	2.903	1.903	2.487	4.202	1.672

These results could be attributed to the close connection of oxygen ions to the B-site ions as well as the A-site ions. Therefore, it might be reasonable to investigate the relationships between oxygen bond valence and TCF for the entire composition of the scheelite compound. The TCF of the specimens was strongly dependent on the oxygen bond valence, as confirmed in Fig. 4. With an increase of oxygen bond valence, the average bond strength of A- and B-site ions could be increased. This in turn, would increased the restoring force for recovering the tilting of A_2BO tetrahedra, and TCF would thereupon decreased.

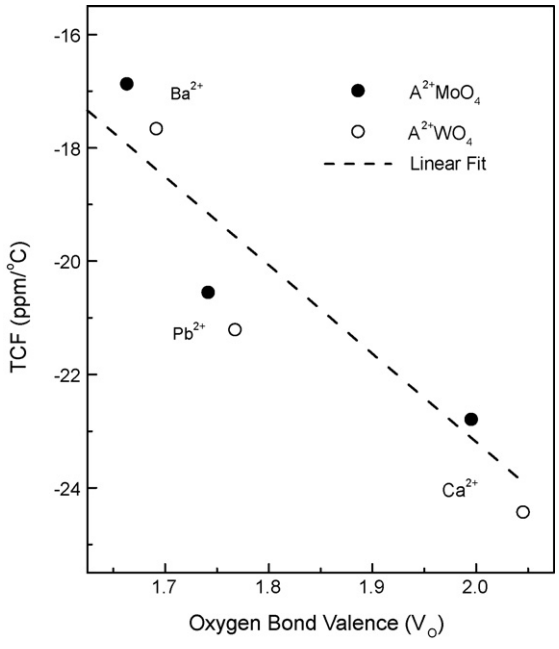

Fig. 4. Dependence of TCF on oxygen bond valence in $A^{2+}B^{6+}O_4$ scheelite compounds.

5. Conclusions

For $A^{2+}B^{6+}O_4$ (A^{2+}: Ca, Pb, Ba; B^{6+}: Mo, W) specimens sintered at 800–1100 °C for 3 h, a single phase with a tetragonal scheelite structure was detected, and the densities of the specimens were higher than the 93% theoretical density for the given composition.

The dielectric constant (K) of $A^{2+}B^{6+}O_4$ scheelite compounds was not only dependent on the ionic polarizability, but also the packing fraction resulting from the effective ionic size and unit cell volume. With the increase of packing fraction from 54% ($BaBO_4$) to 62% ($CaBO_4$), the $Q{\cdot}f$ value increased from 21,620 GHz of $BaWO_4$ to 76,990 GHz of $CaWO_4$. The temperature coefficients of the resonant frequencies (TCF) of the specimens decreased with increasing of oxygen bond valences.

Acknowledgement

This work was partially supported by the Korean-Britain Government Scholarship Programme.

References

1. High-Q LTCC-based passive library for wireless system-on-package (SOP) module development. *IEEE Trans Microwave Theory Tech* 2001;**49**(10):1715.
2. Next generation integral passives: materials, processes, and integration of resistors and capacitors on PWB substrates. *J Mater Sci, Mater Electron* 2000;**11**:253.
3. Lahti M, Lantto V. Passive RF band-pass filters in an LTCC module made by fine-line thick-film pastes. *J Eur Ceram Soc* 1997;**21**:2001.
4. Mohanram A, Lee SH, Messing GL, Green DJ. Constrained sintering of low-temperature co-fired ceramics. *J Am Ceram Soc* 2006;**89**(6):1923.
5. Zheng H, Reaney IM, Muir DM, Price T, Iddles DM. Effect of glass additions on the sintering and microwave properties of composite dielectric

ceramics based on $BaO–Ln_2O_3–TiO_2$ (Ln = Nd, La). *J Eur Ceram Soc* 2007;**27**:4479.
6. Huang CL, Chen HL, Wu CC. Improved high Q value of $CaTiO_3–Ca(Mg_{1/3}Nb_{2/3})O_3$ solid solution with near zero temperature coefficient of resonant frequency. *Mater Res Bull* 2001;**36**:1645.
7. Yoon SH, Choi GK, Kim DW, Cho SY, Hong KS. Mixture behavior and microwave dielectric properties of $(1-x)CaWO_4–xTiO_2$. *J Eur Ceram Soc* 2007;**27**:3087.
8. Seabra MP, Avdeev M, Ferreira VM. Structure–property relations in $xBaTiO_3–(1-x)La(Mg_{1/2}Ti_{1/2})O_3$ solid solutions. *J Am Ceram Soc* 2004;**87**(4):584.
9. Kim ES, Kang DH. Microwave dielectric properties of $(A^{2+}{}_{1/3}B^{5+}{}_{2/3})_{0.5}Ti_{0.5}O_2$ (A^{2+} = Zn, Mg, B^{5+} = Nb, Ta) ceramics. *IEEE Trans Ultrason Ferroelectr Freq Control* 2008;**55**(5):1069.
10. Kim ES, Chun BS. Estimation of microwave dielectric properties of $[(Na_{1/2}La_{1/2})_{1-x}(Li_{1/2}Nd_{1/2})_x]TiO_3$ ceramics by bond valence. *Jpn J Appl Phys* 2004;**43**(1):219.
11. Park HS, Yoon KH, Kim ES. Relationship between the bond valence and the temperature coefficient of the resonant frequency in the complex perovskite $(Pb_{1-x}Ca_x)$ $[Fe_{0.5}(Nb_{1-y}Ta_y)_{0.5}]O_3$. *J Am Ceram Soc* 2001;**84**(1):99.
12. Hakki BW, Coleman PD. A dielectric method of measuring inductive capacitance in the millimeter range. *IRE Trans Microwave Theory Tech* 1960;**8**:402.
13. Nishikawa T, Wakino K, Tanaka H, Ishikawa Y. Precise measurement method for temperature coefficient of microwave dielectric resonator material. *IEEE MTT-S Digest* 1987:277.
14. Galasso FS, Darby W. Structure and properties of inorganic solids. *Int Ser Monogr Solid State Phys* 1970;**7**:106–10.
15. Shannon RD. Revised effective ionic radii and systematic studies of interatomic distances in halides and chalcogenides. *Acta Crystallogr* 1976;**A32**:751.
16. Yoon SH, Kim DW, Cho SY, Hong KS. Investigation of the relations between structure and microwave dielectric properties of divalent metal tungstate compounds. *J Eur Ceram Soc* 2006;**26**:2051.
17. Choi GK, Kim JR, Yoon SH, Hong KS. Microwave dielectric properties of scheelite (A = Ca, Sr, Ba) and wolframite (A = Mg, Zn, Mn) $AMoO_4$ compounds. *J Eur Ceram Soc* 2007;**27**:3063.
18. Kim WS, Kim ES, Yoon KH. Effects of Sm^{3+} substitution on dielectric properties of $Ca_{1-x}Sm_{2x/3}TiO_3$ ceramics at microwave frequencies. *J Am Ceram Soc* 1999;**82**(8):2111.
19. Shannon RD. Dielectric polarizabilities of ions in oxides and fluorides. *J Appl Phys* 1993;**73**(1):348.
20. Brese NE, O'Keefe M. Bond-valence parameters for solids. *Acta Crystallogr* 1991;**B47**:192.